Authors submitted copy

Warm season temperature and summer monsoon history in north-central China since 1740 CE recorded by tree-ring maximum latewood density of Shensi fir

[1]Feng Chen[1, 2 *], Mary H. Gagen[3], Heli Zhang[2], Youping Chen[1], Ziang Fan[2], Fahu Chen[4, 5]

[1] Yunnan Key Laboratory of International Rivers and Transboundary Eco-Security, Institute of International Rivers and Eco-Security, Yunnan University, Kunming, China

[2] Key Laboratory of Tree-ring Physical and Chemical Research of China Meteorological Administration/ Xinjiang Laboratory of Tree-ring Ecology, Institute of Desert Meteorology, China Meteorological Administration, Urumqi, China

[3]Department of Geography, Swansea University, Singleton Park, Swansea SA2 8PP, UK

[4] Key Laboratory of Alpine Ecology, CAS Center for Excellence in Tibetan Plateau Earth Sciences and Institute of Tibetan Plateau Research, Chinese Academy of Sciences (CAS), Beijing 100101, China.

[5] Key Laboratory of Western China's Environmental Systems (Ministry of Education), College of Earth and Environmental Sciences, Lanzhou University, Lanzhou, China.

Abstract Land-surface temperature changes lead to thermal contrasts between the land and the sea and have significant water cycle impacts particularly within global monsoon regions. Whilst such influence may dominate in the East Asian summer monsoon region, impacts on warm-season

*Corresponding author: Feng Chen
E-mail address: feng653@163.com.

temperature dynamics in the East Asian monsoon region have not been effectively explored. Here, an annually resolved maximum latewood density (MXD) record from annual tree rings of Shensi fir (*A. chensiensis*) in the Qinling Mountains (north-central China) provide an East Asian summer monsoon-region relevant 270-year long March-September temperature reconstruction. Our MXD-based temperature reconstruction shows good agreement with phases of observed warming in the 1920s-1950s and 1990s-2000s, a more recent warming hiatus and earlier volcanic-induced cooling phases. Our temperature reconstruction is also significantly correlated with sea surface temperatures in the North Atlantic and reveals linkages between warm season temperature variability in north-central China and the Atlantic Multidecadal Oscillation (AMO). Our warm season temperature reconstruction is sensitive to summer monsoonal season moisture variations in north-central China and provides a multi century perspective on the region's climate which is useful to improving the understanding of monsoonal East Asian climate change and anticipated future extreme drought events in northern China.

Keywords: Qinling Mountains; Temperature reconstruction; East Asian summer monsoon; Volcanic eruptions; Maximum Latewood Density; *Abies chensiensis*

Highlights

A 270-year warm-season temperature reconstruction is developed for the north-central China using maximum latewood density in Shensi fir tree rings (*A. chensiensis*).

Recent summer (March-September) warming exacerbated monsoon season drought in north-central China.

Large-scale volcanic eruptions are correlated with cooler and wetter monsoon years in our reconstruction.

We discuss how the reconstruction informs out understanding of monsoonal East Asian climate change and likely future extreme drought events in northern China.

1. Introduction

Whilst the link between societal and monsoonal stability is historically observable for monsoon regions (Buckley et al. 2010; Pederson et al. 2014; Yang et al. 2014; Liu et al. 2019), exploring the influences of global summer monsoon variability on socioeconomic development and ecosystems is challenging due to spatial and temporal data paucity (Cook et al. 2010; Mohtadi et al. 2016; Tierney et al. 2016). Global climate change has significantly influenced summer monsoon intensity in Asia, and although the ability to simulate the summer monsoon in climate models is improving, there are still great uncertainties in the simulation and prediction of the summer monsoon (Gaetani et al. 2017; Meyer and Jin 2017; Sabeerali and Ajayamohan 2018; Li et al. 2019). Some climate model simulations forecast future increases in monsoonal precipitation in Asia under 21^{st} century climate warming (Hsu et al. 2012; Li et al. 2019) in contrast to observations of declining monsoonal precipitation in northern China and India coincidental with warming and high anthropogenic aerosol forcing over the past 30 years (Liu et al. 2015, 2017; Krishnan et al. 2016; Sandeep et al. 2018; Liu et al. 2019). Such model-observational uncertainty is compounded by the short instrumental records in monsoonal Asia (Douville et al. 2006; Dai and Zhao 2017). In many monsoonal areas climate records are too sparse and only able to provide relatively low spatio-temporal coverage. Climate reconstructions based on tree rings from global monsoonal areas have attempted to contribute to this data paucity and make it possible to describe summer monsoon history, and explore the links between monsoon-drought and relevant modes of atmosphere–ocean circulation (Li et al. 2003, 2019; Bräuning and Mantwill 2004; Singh et al. 2009; Cook et al. 2010; Buckley et al. 2010; Li et al. 2011; Fang et al. 2010, 2012; Griffin et al. 2013; Yang et al. 2014; Baek et al. 2017). Warm-season temperature variability has an important influence on the monsoon-intensity by driving land-sea thermal contrasts (Cook et al. 2013; Tierney et al. 2016; Meyer and Jin 2017; Li et al. 2019). However, to date, few warm-season temperature-sensitive tree-ring latewood maximum density series have been used to expand our picture of temperature and summer monsoon variability in the East Asian middle-low latitude monsoonal regions. Here we address this limit to our current understanding of the past variability of the Asian summer monsoon in north-central China.

As the highest mountain region in eastern China, the Qinling Mountains have a major influence on the climate in monsoonal China and form distinct climatic zones on the range's northern and southern flanks (Lu and Lu 2019). The range is providing new dendroclimatic studies to address climate change in recent centuries (Garfin et al. 2005; Liu et al. 2009, 2014; Chen et al. 2015a) however, to date, no warm-season temperature-sensitive latewood maximum density (MXD) have been explored, despite the proxy's strength in capturing warm season temperatures (Reference needed here). To better understand the mechanisms of climate change in the East Asian monsoon region, a long-term data set, including temperature and precipitation/drought reconstructions is needed. Such long-term perspective is critical for the validation of climate simulations and the integration with other paleoclimate proxy data. The aims of this study were to (1) develop a warm season temperature reconstruction from the Qinling Mountains that improves our understanding of temperature variations in the East Asian middle-low latitude monsoonal region, and (2) to investigate the relationships between reconstructed temperature and the large scale climatology of relevance, and explore the expression of volcanic eruptions in our temperature reconstruction.

2. Materials and methods

2.1. Study area and samples collection

Our study area includes the Guanzhong Plain and the Qinling Mountains regions of north-central China. The region is important in terms of water supply, contributing to China's large-scale South-to-North Water Transfer Project (Li et al, 2015). The Qinling Mountains fall within the Asian monsoon region and are themselves influential, catalysing the formation of distinct climate types on their northern and southern slopes. The climate of the alpine mountain belt (＞1500 m a.s.l.) has 'monsoonal characteristics', and precipitation amounts are plentiful during the summer to early autumn period, snowfall amounts in the winter results in extensive snow coverage.

Our sampling site is situated in the Yinzuishi Provincial Nature Reserve in Zhen'an county in southern Shaanxi (site name - YZY) (Fig. 1). We sampled *A. chensiensis* site from a typical natural Shensi fir forest near the upper treeline with site elevations varrying between 2600 and 2650 m a.s.l. (Table 1). Significant vertical fragmentations occur in the landscape with granite cliffs forming the steep slopes of the sampling site. The vegetation includes Shensi fir (*A. chensiensis)* and bamboo (*Sinarundinaria nitida)*. The soil at the sampling site is shallow and organic rich on granite bedrock. Fifty 10-mm diameter increment cores were taken from twenty-five trees (2 cores per tree) with sampling taking place in 2010.

2.2. MXD chronology development

Ring widths were measured to the nearest of 0.01 mm using a LINTAB measuring system.

First, ring width series were checked using the software COFECHA (Holmes 1983) for possible measurement or dating errors. The cores were cut into 1.0-mm-thin transverse sections using a twin-bladed saw for X-ray densitometry analysis, and an x-ray microdensitometer (DENDRO2003) was used to measure the tree-ring density parameters based on the resultant radiographs. The MXD series were compared to the cross-dating results of ring width series using the DENDRO2003 tree-ring workstation, and COFECHA was used to evaluate any potential cross-dating errors within the MXD value again. In order to remove the growth trends due to site environment, age and size, each individual MXD series was detrended conservatively with a negative exponential, and then the detrended data were combined into the standard YZY MXD chronology (Cook and Kairiukstis 1990). Mean inter-series correlation (Rbar) and the Expressed Population Signal (EPS, Wigley et al. 1984) were used to assess the MXD chronology common signal strength. EPS assesses the relationship between the sample depth and the common signal within a tree-ring chronology, and Rbar is mean correlation between tree-ring series. Standard metrics for acceptable common signal strength were used (Wigley et al, 1984).

2.3. Climate data and statistical analysis

Meteorological stations were selected to explore climate correlations based on distance from station to the sampling site, the observation period, climate data homogeneity and % of missing values. Two stations, Zhen'an and Xi'an, are located in the study area, close to the sampling sites, on the south and north slopes of the Qinling Mountains, respectively (Fig. 1). However, the records of Zhen'an are rather short (1958-2019 CE, 62 years), and Xi'an is the closest station with instrumental data spanning more than 80 years (1932-2019 CE) and a significant correlation ($r \geq$ 0.80) between temperatures of Xi'an and Zhen'an during the period 1958-2019. The climate–tree ring growth correlations were explored between the YZY MXD chronology and monthly and seasonal climate data, include precipitation and temperature, from the Zhen'an and Xi'an climate stations for the common period (1958-2009). Correlation analysis was carried out for a 12-month period from the previous October to the current September. To reveal the relationship between temperature and drought observations, self-calibrating Palmer Drought Severity Index (scPDSI, van der Schrier et al, 2013) data (1958 to 2009) covering the study area (108-109°E, 33-34.5°N) was also used in the climate correlation analysis.

A linear model was used to develop the mean March–September temperature reconstruction using indexed YZY MXD chronology as the predictor. Coefficient of efficiency (CE), reduction of error (RE) and Durbin–Watson statistics were applied to verify our temperature reconstruction using a split-sample climate calibration and leave-one-out cross-validation method (Durbin and Watson, 1950; Michaelsen, 1987; Cook and Kairiukstis 1990). The 1984–2009 period was used for verification, and the 1958–1983 for calibration. RE compares the skill of the reconstruction values with that obtained by using the average instrumental value of the calibration period, and the CE has the same calculation and range and except the CE relies on the average value of the verification period as a baseline of predictive skill, and positive RE and CE indicates useful information in the climate reconstructions (Fritts, 1976). To sure that there is no autocorrelation in the residuals and avoid over-fitting due to the linear trend of temperature, we perform the Durbin–Watson test and calculate the correlation between the first order differences of the sequence, respectively.

To explore the extent to which our temperature reconstruction captures the large-scale temperature variations of central China, we also carried out a correlation analysis between the indexed YZY MXD series and gridded HadCRUT4/HadSST4 temperature data (Cowtan et al. 2014)

(1958–2009). To explore correlation patterns with the relevant large-scale atmospheric circulation, we used the Atlantic Multidecadal Oscillation (AMO, 1856-2009) index from Enfield et al. (2001), the East Asian Summer Monsoon Index (EASMI, 1948-2009) from Li et al. (2010) and the 850mb relative humidity of NCEP Climate Forecast System Reanalysis (CFSR, 1979-2009) from Saha et al. (2010). To explore the linkage between temperature and monsoon drought signals, principal component analysis was used to merge seven monsoon season drought reconstructions based on tree-ring width series from north-central China (Chen et al. 2012, 2013, 2014, 2015b, 2016a, b; Fang et al. 2010, 2012) into a first principal component (PC1), which related to summer monsoon intensity. Cross-wavelet transform of the reconstructed temperature with PC1 was used for applied to evaluate cyclic tendencies in the reconstructions, and the 5% significance level against red noise is shown (Torrence and Compo 1998).

A list of relevant, large volcanic eruption event (Volcanic Explosivity Index (VEI) ≥ 4) years was generated using the volcanic activity chronology from the Smithsonian Institution (http://volcano.si.edu/search_eruption.cfm) (Table 3). Superposed epoch analysis (SEA, Haurwitz and Brier 1981) was used to explore the influences of explosive volcanic eruptions on the YZY MXD temperature reconstruction variability, and drought variation in north-central China based on the stronger volcanic event year lists (VEI ≥ 5). For Granger causality analysis (Attanasio et al., 2012), we employed the natural forcings (total solar irradiance (TSI) (Wang et al., 2005) and cosmic ray intensity (CRI) (Alanko-Huotari et al., 2006), anthropogenic forcings (annual means of CO_2-equivalent concentrations (CO2EQ), Meinshausen et al. 2011; data downloaded from http://www.pik-potsdam.de/~mmalte/rcps/) as well as the climatic indices of influence in the region (Atlantic Multidecadal Oscillation and El Niño-Southern Oscillation (Data available at ftp.ncdc.noaa.gov)).

3. Results

3.1. Relationship between MXD and climatic variables

The standard MXD chronology showed low year-to-year variability, as emphasized low standard deviations (0.099) and standard deviations (0.067). These low values of MXD were found in the previous reports (Schweingruber et al 1978). First-order autocorrelation is 0.47, and implies that climate conditions of previous year tend to carry over their influences on the MXD variation of the following year. High Variance in first eigenvector (VFE, 37%) indicated that the MXD series was responding to common factors. The EPS and Rbar values exceeded 0.85 and 0.50, respectively, prior to the year 1740 CE, and thus, analysis of the resulting temperature reconstruction was truncated prior to 1740 CE.

Correlation analyses between the YZY MXD series and instrumental climate data demonstrates that temperature is positively significant from November to September, covering the whole growth season (Fig. 2a, b). Only one month's precipitation (current April) is negatively significantly correlated with the YZY MXD series. The response of the YZY MXD series to climate on the northern and southern slope of the Qinling Mountains are relatively consistent. Negative correlations were seen between the YZY MXD series and scPDSI in current growing season (Fig. 2c), particularly from July to September. The YZY MXD chronology has the strongest correlations with mean March-September temperature, dominated by the correlation with June to September temperature. The plant physiological behaviour behind this is likely to involve cell division in the cambium halting in the later part of the growing season, to be replaced by thickening of the tracheid cell walls into the early autumn. The correlation is likely to relate to higher temperatures extending the period in which cell wall thickening can occur, resulting in denser latewood (Schweingruber et al, 1978; Yasue et al, 1997). On the other hand, the effect of drought and precipitation in growing season cannot be ignored. Moisture stress during the early growing season (April), is associated with narrow, dense earlywood, and may also associate with higher latewood density. Meanwhile, the negative correlations of PDSI during the monsoonal season suggests that the YZY MXD series is also responsive to summer monsoon droughts. During the weak summer monsoon periods, the precipitation decline and associated rise in temperatures in July–September accelerates the already existing water stress in the early stage, and leads to MXD increases. There is a negative correlation between monsoon drought and temperature in the study area during the instrumental period. Due to the covariance between climate variables, to a certain extent, our MXD data set is also able to capture variability in the monsoon.

3.2. Temperature reconstruction

The period of climatic response (March to September) is long due to the strong influence of the early growing season temperature variations on tree growth. The temperature reconstruction was developed by calibrating the YZY MXD chronology with mean March-September temperature. The YZY MXD index explains 46.2% (r = 0.68) of the instrumental temperature variance during the 1958–2009 period (Fig. 3). We used standard reconstruction tests to assess the reliability of our linear model. Verification tests yielded 0.51 (CE) and 0.41 (RE) for the 1984–2009 verification period, and 0.15 (CE) and 0.20 (RE) for the 1958–1983 verification period, indicating the good reliability of our temperature model. Both the RE (0.42) and CE (0.41) are also strongly positive, and the correlation is 0.65 using leave-one-out method validation. The Durbin–Watson test (1.31, P <

0.001) reveals no substantial autocorrelation in the residuals for the full period. The first differences of the MXD series explained 25% of the actual variances. For the longer instrumental period (1932-2009), the estimated data showed a good agreement (r = 0.62, P < 0.01) with the Xi'an observed temperature.

3.3. The reconstructed temperature record, 1740–2009

The reconstruction revealed valuable information on the temperature variability of this border area between southern and northern China, for the 1740–2009 period. The long term mean of the reconstruction is 0.2°C warmer than the instrumental period average for 1958–2009. The coldest warm season years are in 1786 and 1976 (both -1.3°C) and 1970 (-1.2°C). The warmest warm season years are in 1831, 1744 and 1928 (+0.9°C). Some high temperature years are closely related to extreme drought events, such as 1843-1844 burning summer and 1928 drought (Zhang et al. 2004; Liang et al. 2006). Evidence for two pronounced warm periods in the twentieth century, and the recent warming slowdown is also found. The warming rate in the 1998-2009 period (-0.1℃/10a) was significantly lower than (0.4℃/10a) that in the 1980-2009 period, and meanwhile, the warming rate recorded by tree rings in the natural state is also lower than that (0.8℃/10a) in the climate stations of the plain cities (Xi'an and Zhen'an). Temperatures are relatively high at the start of the reconstruction and then, from the middle of the 18th century begin to fall, reaching one of the lowest temperature points in the record, in the period from 1770-1790. High temperatures were recorded during the 1800s–1850s, and relatively low temperatures were recorded during the 1860s–1890s. Notable depressions in the 1780s-1790s and 1810s-1820s may be linked with major volcanic eruptions (Hao et al. 2014; Anchukaitis et al. 2012). The reconstructed temperature changes of the 20th century show the first warming period from the middle 1920s to the early 1950s and the second warming period from the early 1990s to the present. Reconstructed low-frequency temperature variations including the cold period of the 1960-1970s are consistent with the temperature variations reported from the instrumental Sea Surface Temperature (SST, Rayner et al. 2003) observations and the European summer temperature reconstructions based on the MXD data (Büntgen et al. 2008).

In exploring spatial correlations with gridded temperature data (HadCRUT4/HadSST4, Fig. 5a) significant correlation areas were found on both the northern and southern sides of the Qinling Mountains and in the Huai River basin, with the strongest correlations occurring in the Qinling Mountain area, Shaanxi (Fig. 5a). The results reveal that large-scale warm season temperature signals across north-central China are captured by the YZY MXD warm season temperature reconstruction. The temperature reconstruction is negatively correlated with CFSR 850mb relative humidity and precipitation (Fig. 5b, c). Since the AMO has some important effects on the summer temperature of the East Asian continent (Li and Luo 2013), we screened our temperature reconstruction in the correlation analysis with various lags of monthly and seasonal AMO index values (Enfield et al. 2001) for the period 1856-2009. The highest correlation (r = 0.32, P < 0.01) was found between the previous October-September AMO index and our reconstruction and increased to 0.61 after 20-yr smoothing during the period 1856-2009 (Fig. 5d). A comparison between our reconstruction and EASMI reveals no significant linkage, and even if the two series are transformed to the first differences, the coherence is still relatively weak (r = 0.27, P<0.05) between the two series. However, the relatively low correlations with the EASMI in the 1950s-1970s strengthen until there is high coherence with the temperature reconstruction in the 1980s-2000s (r = 0.42, P<0.01) (Fig. 5e), and correlation between the first order differences is 0.60 (P< 0.01).

Several studies point to a monsoon region volcanic response of wet and cool condition following large volcanic eruptions (Anchukaitis et al, 2010; Zuo et al, 2019). Thus, comprehensive research on regional climate change responses to volcanic eruptions based on tree-ring width and MXD series would help us better understand the impacts of volcanic eruptions on the climate of northern China. A comparison between our reconstruction and large volcanic eruptions via the volcanic explosivity index (VEI ≥ 5) reveals that cooling is evidenced during the event year or the following year (Fig. 6). Detailed superposed epoch analysis (SEA) (Haurwitz and Brier, 1981) also provides evidence that volcanic eruptions caused cooling effects, and cooling (-0.56℃) occurred during the year of volcanic eruption events (1755, 1783, 1815, 1822, 1835, 1883, 1902, 1955, 1963, 1982, 1986); similarly, there is extraordinary cooling (-0.65℃) the year following volcanic eruption events (1741, 1800, 1843, 1886, 1912, 1916, 1933, 1991) (Fig. 5a). In addition, other examples of volcanic induced cooling (VEI= 4) were also found (Table 2). Volcanic eruptions in the High and mid-latitude areas (＞30°N) had a greater impact on the temperature in Central Asia (−0.76 °C) than volcanic eruptions in Low-latitude areas (≤ 30°N) and southern hemisphere (−0.67 °C). Based on the SEA results between the large volcanic events (VEI ≥ 5) and the PC1 (38.5-48.5%) of the drought reconstructions in north-central China (Fang et al, 2010, 2012; Chen et al, 2012, 2013, 2014, 2015b, 2016a, b), we found that the relatively wet condition were also indicated in our reconstruction, following major volcanic eruptions (Fig. 6b).

4. Discussion

4.1 The evaluation of the 20th century warm periods

Both instrumental climate data series used in this study record warming associated with anthropogenic climate change in the 20^{th} century. The change in average temperature from 1958-

1968 to 2008-2018 is 1.7 °C in the Zhen'an record and 1.5 °C in the Xi'an record. The pattern of change through the 20th century reveals two relatively warm periods (1920s–40s and 1990s–present) separated by a relatively cool period (1950s–70s) (Li et al, 2017; Soon et al, 2018) with recent warm season temperature in the instrumental record higher than at any point in the last 240 years. Whilst the scarcity of long instrumental records has given rise to debate about how these two warm periods compare to each other. The high-resolution proxy data becomes an important way to make up for the lack of instrumental climate data, and our reconstruction indicates that of the two sustained warm periods in the 20th century (1923–1952 and 1993–2009) the latter (0.4 °C) is warmer than the former (0.2 °C), and instrumental temperature data from Zhen’an and Xi’an even reached at 0.8°C and 0.9 °C, in contrast to Soon et al (2018). Granger causality analysis indicate that human activities, such as greenhouse gas emission and rapid urbanization, have played an important role in recent climate warming in the region (Li et al, 2018) (Table 3). In the instrumental and reconstructed temperature data of 1993 to 2019, although north-central China is still much warmer than the long term mean, there is a slowdown of warming in the summer 1998–2015 (Fig. 5c). The warm season temperature, at significant lows in the 2005–2014 period, appears to have significantly and rapidly increased after 2014. Such changes in the rate of regional background warming are well within model ranges and can be expected to continue as global average background temperatures continue to increase (Lewandowsky et al. 2015). The recent warming period in the region resembles the trends in the 1920s-1940s, suggesting that the 20th century second warm period is still going on. A continued increase in temperature for the late 2010s is further supported by the higher temperature from 2015 to 2019, at 1.6 and 1.1°C above the mean temperature for 1958–2019 and the lack of a cold year between 2015 and 2019. As a result of the resumption of a faster rate of summer warming in recent years, the warming trend in the border area between southern and northern China is also a concern. Granger causality analysis also revealed that AMO have some influences in climate warming during the 20th century (Table 3). Thus, higher SSTs in the Arctic and North Atlantic Oceans and the positive phase of the AMO (Monerie et al, 2018; Gervais et al, 2019) may suggest that the warming trend will be further aggravated, promoting the northward movement of the subtropical boundary and monsoon rain belt of China with potentially profound impacts on water resources across the region.

4.2 Influences of temperature and volcanic eruption on East Asian monsoon

We carried out a correlation analysis between the YZY MXD reconstruction and SSTs in the Arctic and North Atlantic Oceans and the European warm season temperature (Zampieri et al, 2017; Årthun et al, 2018) are found (Fig. 5a). The resultant correlations suggested a possible connection with the SSTs changes in the middle and high latitudes of the Northern Hemisphere (Sun et al, 2018; Monerie et al, 2018, 2019; Zhang et al, 2020). Positive correlations with the AMO would indicate that temperatures in north-central China were relatively high when strong warming occured in the mid-high latitude North Atlantic and Arctic oceans, especially in the two twentieth-century warm periods, and this may be linked with the influence of Arctic amplification (Vavrus, 2018; Huang et al., 2019). Anomalous warming in the Atlantic Ocean has warmed the upper and middle troposphere in the Northern Hemisphere, leading to temperature increases in Eurasia, including eastern China (Wang et al, 2009; Wang et al, 2013; Monerie et al, 2018; Zhang et al, 2020), and the AMO signals have also been recorded in the tree rings of the high altitude mountains of north-central China. In addition, the differences between onset time and magnitude of the two twentieth-century warming events and the AMO variations may be linked with drought-induced warming, including the drought period in late 1920s and the decline in monsoonal precipitation since the 1980s (Liang et al, 2006; Fang et al, 2010, 2012; Chen et al, 2013).

Of particular interest is the strengthened correlation between our YZY MXD temperature reconstruction and EASMI under the recent warm conditions. Accompanying the positive AMO phase, the SST anomaly is positive over the adjacent oceans of the East Asian domain, which generates an early start of the rainy seasons of the Yangtze River basin, and the enhanced Western Pacific Subtropical High expanded westward and northward (Zhou et al, 2009a; Li et al, 2010; Kim and Kim, 2010). Since our study area is adjacent to the middle-lower reaches of the Yangtze River where the EASMI exhibits greatest sensitivity, the correlation may be associated with the positional change of the East Asian monsoon in the context of recent accelerated warming (Li et al, 2010; Gao et al, 2014). However, during the last 30 years, 850mb relative humidity in the study area has decreased. The comparison of PC1 and the YZY MXD temperature reconstruction (r =0.31, $P < 0.01$) shows that positive temperature anomalies during March-September tend to be followed by an anomalous deficit of precipitation over central-north China in the summer monsoon season, while negative temperature anomalies tend to be followed by relatively high precipitation, such as the most severe droughts in late 1920s-1930s (Fig. 7a). Furthermore, the coherence between the temperature reconstruction and PC1 has varied in time across most spectral bands, and shows significant antiphase changes (Fig. 7b). Therefore, for north-central China, the the enhanced synchronism does not necessarily mean increased summer monsoon intensity (high precipitation) (Zhou et al, 2009b; Li et al, 2010), and on the contrary, the attenuation of water vapor carried by the EASM is significant (Fig. 5c), and the precipitation in the north of the study area is greatly reduced, while evaporation increases with the rise in warm season temperatures, exacerbating drought stress, and aridification in the recent warming period. Correlations between PC1 and the PDSI series (35.5-39.5°N, 100.5-111.00°E) extracted from the Monsoon Asia Drought Atlas (Cook et al. 2010), computed over the 1740–2005 common period, is 0.45 ($P < 0.01$), and both show a significant drying trend over the past 30 years in the northern monsoon fringe of north-central China. At the same time, a negative correlation (r =0.41, $P < 0.01$) was found between low-frequency changes of PC1 and the EASMI (Wang and Fan 1999) calculated based on the NCAR's Community Climate System Model 4 (CCSM4) data (Fig. 7c), and this may be linked with the north-south contrasting pattern of summer precipitation variations over eastern China. However, there is no positive correlation between the EASMI and the temperature reconstruction, and on the contrary, some out-of-phase relationships between the EASMI and the temperature reconstruction were found before the recent warming period (Fig. 7d). This implied that the simulation capability for the temperature change in the region may needs to be improved although the simulation results may have a good indication for the drought change in the East Asian monsoon region, and meanwhile, it is also necessary to establish more reliable temperature series in the East Asian monsoon region in order to reveal the past temperature change more accurately. Recent drying trends have been found in surrounding areas, and an out-of-phase relationship between our reconstructed temperature and the moisture-sensitive tree-ring width series from Mongolian Plateau (Hessl et al., 2018) was found (Fig. 8). In the past 30 years, a remarkable warming and drying trend occurred synchronously at north-central China and Mongolian Plateau, and the warming and drying trend in Mongolia is becoming more and more obvious (Hessl et al. 2018; Liu et al. 2019). This indicates the effects of the warming and drying are not confined to northern China, but have even affected Mongolian Plateau. The result also resembles other findings in the North American monsoon area (Pascale et al, 2017) and suggests continued rising global background temperatures and its associated potential drought events may have significant impacts for the poleward edge of the EASM domain (Huang et al., 2017).

In response to investigations of the regional impact of large scale volcanic eruptions we find a shift of the cooling year in year 0 (the eruption year) to year 1 (Fig. 6a), variable with the location and season of the volcanic eruption and the atmospheric circulation at the time (Hao et al, 2014). Volcanic eruptions in the Pacific rim played an important role in volcanic cooling, especially in the Philippines, Indonesia and Japan (Table 2). The complicated and volatile Asian summer monsoon system with high interannual variations, however, may lead to a high response of tree-ring density, because the cooling influence lasts for only a short, but significant, time (Esper et al, 2013). This unusual volcanic cooling can also significantly affect the intensity of the summer monsoon with an increase in humidity in the north-central China in the year following the volcanic eruptions, sometimes persisting for 2–4 more years (Fig. 6b). The wetter condition in north-central China after the volcanic eruptions is caused by enhanced cross-equator flow (Anchukaitis et al. 2012; Zuo et al, 2019), but also may be related to the decrease of evaporation due to low temperatures. However, because of the relatively short duration of this effect, it does not fundamentally change the region's arid background climate.

5. Conclusion

In this study, a 270-year March–September temperature reconstruction for the north-central China is developed based on the MXD series of *A. chensiensis* from the Qinling Mountains. The temperature reconstruction reflects the large-scale temperature variations of north-central China, despite complex and varied geographic conditions and spatial differences in local climate change. Large scale controls on regional temperature variation not only reflect complex ocean–atmosphere–land circulation and thermodynamic impacts with great spatiotemporal variations but are also related to the external forcings, such as periodic volcanic eruptions. We suggest that two twentieth-century significant warming episodes have occurred in the Qinling Mountains, even though the recent warming rate slowed down (to 2015). The cooling and warming trends indicated by the tree-ring MXD data of the Qinling Mountains are in good agreement with AMO variability during the period 1857-2009 and suggest that warm season temperature fluctuations in north-central China may have connections with the climate of the North Atlantic and Arctic Oceans. Post-eruption cooling and wetting responses to large volcanic eruptions were found in our reconstruction based on the results of the superposed epoch analysis. If climate warming continues at its current accelerated rate, as seems likely, warm season temperatures in the Qinling Mountains are likely to continue to rise in line with background warming, and water resource allocation and the social and economic systems in the north-central China will need careful adaptation.

Acknowledgments

This research was supported by the National Key R&D Program of China (2018YFA0606401) and NSFC (U1803341).

References

Alanko-Huotari K, Mursula K, Usoskin IG, Kovaltsov GA (2006) Global heliospheric parameters and cosmic-ray modulation: an empirical relation for the last decades. Solar Physics 238: 391-404.

Anchukaitis KJ, Buckley BM, Cook ER, Coo BI, D'Arrigo RD, Ammann CM (2010) Influence of volcanic eruptions on the climate of the Asian monsoon region. Geophy Res Lett 37: L22703

Anchukaitis KJ, Breitenmoser P, Briffa KR, Buchwal A, Büntgen U, Cook ER, D’Arrigo RD, Esper

J, Evans MN, Frank D, Grudd H, Gunnarson BE, Hughes MK, Kirdyanov AV, Korner C, Krusic PJ, Luckman B, Melvin TM, Salzer MW, Shashkin AV, Timmreck C, Vaganov EA, Wilson RJS (2012) Tree rings and volcanic cooling. Nat Geosci 5(12):836–837

Årthun M, Kolstad EW, Eldevik T, Keenlyside NS (2018) Time scales and sources of European temperature variability. Geophy Res Lett 45(8): 3597-3604

Attanasio A, Pasini A, Triacca U (2012) A contribution to attribution of recent global warming by out-of-sample Granger causality analysis. Atmospheric Science Letters, 13(1), 67-72.

Baek SH, Smerdon JE., Coats S, Williams AP, Cook BI, Cook ER, Seager R (2017) Precipitation, temperature, and teleconnection signals across the combined North American, monsoon Asia, and Old World drought atlases. J Clim 30(18): 7141-7155.

Bräuning A, Mantwill B (2004) Summer temperature and summer monsoon history on the Tibetan plateau during the last 400 years recorded by tree rings. Geophy Res Lett 31(24).

Buckley BM, Anchukaitis KJ, Penny D, Fletcher R, Cook ER, Sano M, Nam LC, Wichienkeeo A, Minh TT, Hong TM (2010) Climate as a contributing factor in the demise of Angkor, Cambodia. Proc Natl Acad Sci USA 107:6748–6752

Büntgen U, Frank D, Grudd H, Esper J (2008) Long-term summer temperature variations in the Pyrenees. Clim Dyn 31(6): 615-631

Chen F, Yuan YJ, Wei WS, Yu SL, Fan ZA, Zhang RB, Zhang TW, Shang HM (2012) Tree-ring-based reconstruction of precipitation in the Changling Mountains, China, since AD 1691. Int J Biometeorol 56(4): 765-774

Chen F, Yuan YJ, Wei WS, Fan ZA, Yu SL, Zhang TW, Zhang RB, Shang HM, Qin L (2013) Reconstructed precipitation for the north-central China over the past 380 years and its linkages to East Asian summer monsoon variability. Quat Int 283: 36-45.

Chen F, Yuan Y, Zhang R, Qin L (2014) A tree-ring based drought reconstruction (AD 1760–2010) for the Loess Plateau and its possible driving mechanisms. Global Planet Change 122: 82-88

Chen F, Zhang RB, Wang HQ, Qin L (2015a) Recent climate warming of central China reflected by temperature-sensitive tree growth in the eastern Qinling Mountains and its linkages to the Pacific and Atlantic oceans. J Mountain Sci 12(2): 396-403

Chen F, Yuan Y, Wei W, Fan Z, Zhang R, Yu S (2015b) April–June precipitation reconstruction for Xi'an and drought assessment for the Guanzhong Plain from tree rings of Chinese pine. J Water

Clim Change 6(3): 638-646

Chen F, Yuan Y, Zhang T, Linderholm HW (2016a) Annual precipitation variation for the southern edge of the Gobi Desert (China) inferred from tree rings: linkages to climatic warming of twentieth century. Nat Haza 81(2): 939-955

Chen F, Zhang R, Wang H, Qin L, Yuan Y (2016b) Updated precipitation reconstruction (AD 1482–2012) for Huashan, north-central China. Theor Appl Climatol 123(3-4): 723-732

Cook ER, Kairiukstis LA (Eds.) (1990), Methods of Dendrochronology, Springer, New York

Cook ER, Anchukaitis KJ, Buckley BM, D’Arrigo RD, Jacoby GC, Wright WE (2010) Asian monsoon failure and megadrought during the last millennium. Science, 328, 486-489

Cook ER, Krusic PJ, Anchukaitis KJ, Buckley BM, Nakatsuka T, Sano M (2013) Tree-ring reconstructed summer temperature anomalies for temperate East Asia since 800 CE. Clim Dyn 41(11-12): 2957-2972

Cowtan K, Way RG (2014) Coverage bias in the HadCRUT4 temperature series and its impact on recent temperature trends. Q J Roy Meteorol Soc 140(683): 1935-1944

Dai A, Zhao T (2017) Uncertainties in historical changes and future projections of drought. Part I: estimates of historical drought changes. Clim Change 144(3): 519-533

Diebold FX, Mariano RS. 1995. Comparing predictive accuracy. J Bus Econ Stat 13: 253–265.

Douville H, Salas-Mélia D, Tyteca S (2006) On the tropical origin of uncertainties in the global land precipitation response to global warming. Clim Dyn 26(4): 367-385

Durbin J, Watson GS (1950) Testing for serial correlation in least squares regression: I. Biometrika, 37(3/4): 409-428

Enfield DB, Mestas-Nuñez AM, Trimble PJ (2001) The Atlantic multidecadal oscillation and its relation to rainfall and river flows in the continental US. Geophy Res Lett 28(10): 2077-2080

Fang KY, Gou XH, Chen FH, D'Arrigo R, Li J (2010) Tree-ring based drought reconstruction for the Guiqing Mountain (China): linkages to the Indian and Pacific Oceans. Int J Climatol 30(8): 1137-1145

Fang K, Gou X, Chen F, Liu C, Davi N, Li J, Zhao Z, Li Y, Fang K, Gou X, Chen F, Liu C, Davi N, Li J, Zhao Z, Li Y (2012) Treering based reconstruction of drought variability (1615–2009) in the Kongtong Mountain area, northern China. Global Planet Change 80–81:190-197

Fritts HC (1976) Tree rings and climate. The Blackburn Press, Caldwell

Gaetani M, Flamant C, Bastin S, Janicot S, Lavaysse C, Hourdin F, Braconnot P, Bony S (2017)

West African monsoon dynamics and precipitation: the competition between global SST warming and CO_2 increase in CMIP5 idealized simulations. Clim Dyn 48:1353-1373

Gao H, Jiang W, Li W (2014) Changed relationships between the East Asian summer monsoon circulations and the summer rainfall in eastern China. J Meteorol Res 28(6): 1075-1084

Garfin GM, Hughes MK, Yu L, Burns JM, Touchan R, Leavitt SW, An ZS (2005) Exploratory temperature and precipitation reconstructions from the Qinling Mountains, north-central China. Tree-ring Res 61(2): 59-72

Gervais M, Shaman J, Kushnir Y (2019) Impacts of the North Atlantic Warming Hole in Future Climate Projections: Mean Atmospheric Circulation and the North Atlantic Jet. J Clim 32(10): 2673-2689

Granger CWJ, Newbold P. 1997. Forecasting Economic Time Series. Academic Press: New York, NY.

Griffin D, Woodhouse CA, Meko DM, Stahle DW, Faulstich HL, Carrillo C, Touchan R, Castro CL, Leavitt SW (2013) North American monsoon precipitation reconstructed from tree-ring latewood. Geophys Res Lett 40:954–958. doi:10.1002/grl.50184

Hao Z, Wang H, Zheng J (2014) Spatial and temporal distribution of large volcanic eruptions from 1750 to 2010. J Geogr Sci 24(6): 1060-1068.

Haurwitz MW, Brier GW (1981) A critique of the superposed epoch analysis method: its application to solar–weather relations. Mon Weather Rev 109(10): 2074-2079

Hessl AE, Anchukaitis KJ, Jelsema C et al (2018) Past and future drought in Mongolia. Sci Adv 4(3):e1701832

Kim KY, Kim BS (2020) The effect of regional warming on the East Asian summer monsoon. Clim Dyn 54: 3259–3277.

Kosaka Y, Xie SP (2013) Recent global-warming hiatus tied to equatorial Pacific surface cooling. Nature 501: 403-407.

Holmes RL (1983) Computer-assisted quality control in tree-ring dating and measurement. Tree-ring Bull 43: 69-78

Huang J, Yu H, Dai A, Wei Y, Kang L (2017) Drylands face potential threat under 2 C global warming target. Nat Clim Change 7(6): 417-422

Huang J, Ou T, Chen D, Luo Y, Zhao Z (2019) The amplified Arctic warming in the recent decades may have been overestimated by CMIP5 models. Geophy Res Lett 46(22): 13338-13345.

Li J, Wu Z, Jiang Z, He J (2010) Can global warming strengthen the East Asian summer monsoon?. J Clim 23(24): 6696-6705

Hsu PC, Li T, Luo JJ, Murakami H, Kitoh A, Zhao M (2012) Increase of global monsoon area and precipitation under global warming: A robust signal?. Geophy Res Lett 39: L06701

Krishnan R, Sabin TP, Vellore R, Mujumdar M, Sanjay J, Goswami BN, Hourdin E, Dufresse J-L, Terray P (2015) Deciphering the desiccation trend of the south Asian monsoon hydroclimate in a warming world. Clim Dyn 47(3):1007-1027

Lewandowsky S, Risbey JS, Oreskes N (2015) On the definition and identifiability of the alleged “hiatus” in global warming. Sci Rep 5(1): 1-13.

Liang EY, Liu X, Yuan Y, Qin N, Fang X, Huang L, Zhu H, Wang L, Shao X (2006) The 1920s drought recorded by tree rings and historical documents in the semi-arid and arid areas of northern China. Clim Change 79(3-4), 403-432.

Li G, Zhang X, Mirzaei PA, Zhang J, Zhao Z (2018) Urban heat island effect of a typical valley city in China: responds to the global warming and rapid urbanization. Sustain Cities Soc 38: 736-745

Li SL, Luo FF (2013) Lead-lag connection of the Atlantic Multidecadal Oscillation (AMO) with East Asian surface air temperatures in instrumental records. Atmos Oceanic Sci Lett 6(3): 138-143

Li QX, Zhang L, Xu, W, Zhou T, Wang J, Zhai P, Jones P (2017) Comparisons of time series of annual mean surface air temperature for china since the 1900s: Observations, model simulations, and extended reanalysis. Bull Amer Meteorol Soc 98(4): 699-711

Li Q, Nakatsuka T, Kawamura K, Liu Y, Song H (2011) Hydroclimate variability in the North China Plain and its link with El Niño–Southern Oscillation since 1784 AD: Insights from tree-ring cellulose δ18O. J Geophy Res: Atmos 116(D22)

Li J, Wu, Z, Jiang, Z, He J (2010) Can global warming strengthen the East Asian summer monsoon?. J Clim 23(24): 6696-6705

Li L, Zhang L, Xia J, Gippel CJ, Wang R, Zeng S (2015) Implications of modelled climate and land cover changes on runoff in the middle route of the south to north water transfer project in China. Water Resour Manag 29(8): 2563-2579

Li Z, Sun Y, Li T, Ding Y, Hu T (2019) Future Changes in East Asian Summer Monsoon Circulation and Precipitation Under 1.5 to 5°C of Warming. Earth's Future 7(12): 1391-1406

Liu J, Chen J, Zhang X, Li Y, Rao Z, Chen, FH (2015) Holocene East Asian summer monsoon records in northern China and their inconsistency with Chinese stalagmite δ18O records. Earth-Sci Rev 148: 194-208

Liu J, Rühland KM, Chen J, Xu Y, Chen S, Chen Q, Huang W, Xu Q, Chen F, Smol JP (2017) Aerosol-weakened summer monsoons decrease lake fertilization on the Chinese Loess Plateau. Nat Clim Change 7: 190-194

Liu Y, Linderholm HW, Song HM, Cai QF, Tian QH, Sun JY, Chen DL, Simelton E, Seftifen K, Tian H, Wang RR, Bao G, An ZS (2009) Temperature variations recorded in Pinus tabulaeformis tree rings from the southern and northern slopes of the central Qinling Mountains, central China. Boreas 38:285-291

Liu Y, Wang YC, Li Q, Song HM, Linderhoim HW, Leavitt SW, Wang RY, An ZS (2014) Tree-ring stable carbon isotope-based May–July temperature reconstruction over Nanwutai, China, for the past century and its record of 20th century warming. Quat Sci Rev 93:67-76

Liu Y, Cai W, Sun C, Song H, Cobb K M, Li J, Leavitt S W, Wu L, Cai Q, Liu R, Ng B, Cherubini P, Büntgen U, Song Y, Wang G, Lei Y, Yan L, Li Q, Ma Y, Fang C, Sun J, Li X, Chen D, Linderholm H W. 2019b. Anthropogenic aerosols cause recent pronounced weakening of Asian Summer Monsoon relative to last four centuries. Geophys Res Lett, 46: 5469–5479

Lu FZ, Lu HY (2019) A high-resolution grid dataset of air temperature and precipitation for Qinling-Daba Mountains in central China and its implications for regional climate. Acta Geogr Sin 74: 875-888

Meinshausen M, Smith S, Calvin K et al (2011) The RCP greenhouse gas concentrations and their extensions from 1765 to 2300. Clim Change 109: 213–241

Meyer JD, Jin J (2017) The response of future projections of the North American monsoon when combining dynamical downscaling and bias correction of CCSM4 output. Clim Dyn 49(1-2): 433-447

Michaelsen J (1987) Cross-validation in statistical climate forecast models. J Clim Appl Meteorol 26(11): 1589-1600

Monerie PA, Robson J, Dong B, Dunstone N (2018) A role of the Atlantic Ocean in predicting summer surface air temperature over North East Asia?. Clim Dyn 51(1-2): 473-491

Monerie PA, Robson J, Dong B, Hodson DL, Klingaman NP (2019) Effect of the Atlantic multidecadal variability on the global monsoon. Geophy Res Lett 46(3): 1765-1775

Mohtadi M, Prange M, Steinke S (2016) Palaeoclimatic insights into forcing and response of monsoon rainfall. Nature 533(7602): 191-199

Pascale S et al (2017) Weakening of the North American monsoon with global warming. Nat Clim Change 7: 806-812

Pederson N, Hessl AE, Baatarbileg N, Anchukaitis KJ, Di Cosmo N (2014) Pluvials, droughts, the Mongol Empire, and modern Mongolia. P Nat Acad Sci 111(12): 4375-4379

Rayner N, Parker D, Horton E, Folland C, Alexander L, Powell D (2003) Global analyses of SST, sea ice and night marine air temperature since the late nineteenth century. J Geophys Res 108. doi:10.1029/2002JD002670

Sabeerali CT, Ajayamohan RS (2018) On the shortening of Indian summer monsoon season in a warming scenario. Clim Dyn 50(5-6): 1609-1624

Sandeep S, Ajayamohan RS, Boos WR, Sabin TP, Praveen V (2018) Decline and poleward shift in Indian summer monsoon synoptic activity in a warming climate. P Nat Acad Sci USA 115(11): 2681-2686

Schweingruber FH, Fritts HC, Bräker OU, Drew LG, Schär E (1978) The X-ray technique as applied to dendroclimatology. Tree-Ring Bull 38:61–91

Singh J, Yadav RR, Wilmking M (2009) A 694-year tree-ring based rainfall reconstruction from Himachal Pradesh, India. Clim Dyn 33(7-8): 1149-1158

Soon WWH, Connolly R, Connolly M, O'Neill P, Zheng J, Ge Q, Yan H (2018) Comparing the current and early 20th century warm periods in China. Earth Sci Rev 185:80-101

Sun X, Li S, Hong X, Lu, R (2019) Simulated influence of the Atlantic multidecadal oscillation on summer eurasian nonuniform warming since the mid-1990s. Adv Atmos Sci 36(8): 811-822

Tierney JE, Pausata FS, Demenocal P (2016) Deglacial Indian monsoon failure and North Atlantic stadials linked by Indian Ocean surface cooling. Nature Geosci 9(1): 46-50

Torrence C, Compo GP (1998) A practical guide to wavelet analysis. Bull Am Meteorol Soc 79:61–78

van der Schrier G, Barichivich J, Briffa KR, Jones PD (2013) A scPDSI-based global data set of dry and wet spells for 1901–2009. J Geophy Res: Atmos 118(10): 4025-4048

Vavrus SJ (2018). The influence of Arctic amplification on mid-latitude weather and climate.

Current Clim Change Rep 4(3): 238-249.

Wang B, Fan Z (1999) Choice of South Asian summer monsoon indices. Bull Amer Meteor Soc 80: 629-638.

Wang YM, Lean JL, Sheeley Jr NR (2005) Modeling the Sun’s magnetic field and irradiance since 1713. The Astrophysical J, 625(1): 522-538.

Wang Y, Li S, Luo D (2009) Seasonal response of Asian monsoonal climate to the Atlantic Multidecadal Oscillation. J Geophy Res: Atmos 114(D2)

Wang J, Yang B, Ljungqvist FC, Zhao Y (2013) The relationship between the Atlantic Multidecadal Oscillation and temperature variability in China during the last millennium. J Quat Sci 28(7): 653-658

Wigley T, Briffa KR, Jones PD (1984) On the average value of correlated time series, with applications in dendroclimatology and hydrometeorology. J Clim Appl Meteorol 23:201-213

Wu R, You T, Hu K (2019) What formed the north-south contrasting pattern of summer rainfall changes over eastern China?. Current Clim Change Rep 5(2): 47-62.

Yang B, Kang S, Ljungqvist FC, He MH, Zhao Y, Qin C (2014) Drought variability at the northern fringe of the Asian summer monsoon region over the past millennia. Clim Dyn 43(3-4): 845-859.

Zampieri M, Toreti A, Schindler A, Scoccimarro E, Gualdi S (2017) Atlantic multi-decadal oscillation influence on weather regimes over Europe and the Mediterranean in spring and summer. Global Planet Change 151: 92-100.

Zhang DE, Gaston D (2004) Northern China maximum temperature in the summer of 1743: A historical event of burning summer in a relatively warm climate background. Chin Sci Bull 49: 2508-2514

Zhang G, Zeng G, Li C, Yang X (2020) Impact of PDO and AMO on interdecadal variability in extreme high temperatures in North China over the most recent 40-year period. Clim Dyn 54(5) 3003-3020

Zhou T, Gong D, Li J, Li B (2009a) Detecting and understanding the multi-decadal variability of the East Asian Summer Monsoon–Recent progress and state of affairs. Meteorol Z 18(4): 455-467

Zhou T, Yu R, Zhang J, Drange H, Cassou C, Deser C, Hodson D, Sanchez-Gomez E, Li J, Keenlyside N, Xin X, Okumura Y (2009b) Why the western Pacific subtropical high has extended westward since the late 1970s. J Clim 22(8): 2199-2215

Zuo M, Zhou T, Man WM (2019) Wetter global arid regions driven by volcanic eruptions. J Geophy Res: Atmos 124: 13648-13662

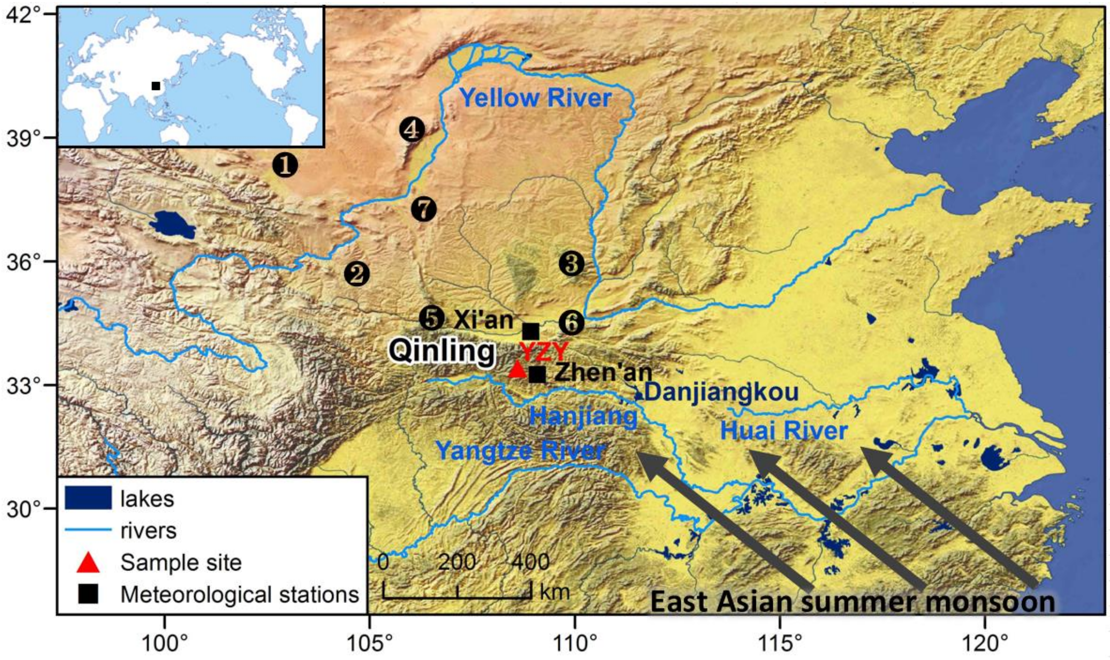

Fig. 1 Map showing the locations of sampling site and meteorological stations mentioned in text. The regions 1, 2, 3, 4, 5, 6 and 7 indicate the tree-ring sites of Chen et al., 2012, Fang et al., 2010, Chen et al., 2014, Chen et al., 2016a, Fang et al., 2012, Chen et al., 2013 and Chen et al., 2016b, respectively.

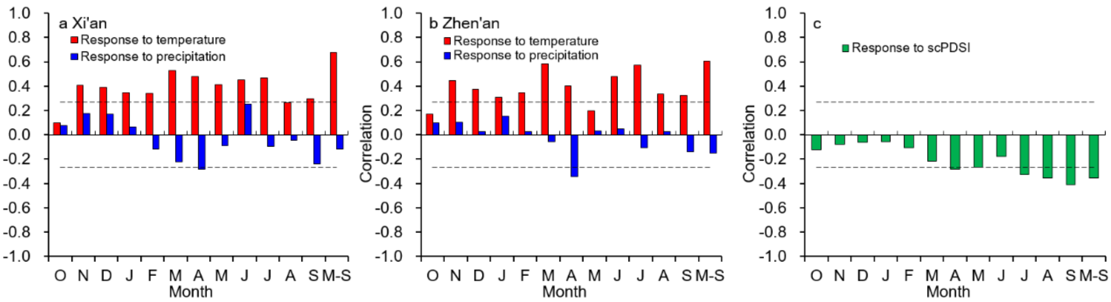

Fig. 2 Correlation coefficients between the MXD chronology and climate factors at the Xi'an (a) and Zhen'an (b). (c) Correlation coefficients between the MXD chronology and scPDSI (van der Schrier et al, 2013). Correlations were calculated from previous October to September, as well as the seasonal means (March-September), over the 1958–2009 common period. Horizontal dashed lines denote the 95% confidence limits.

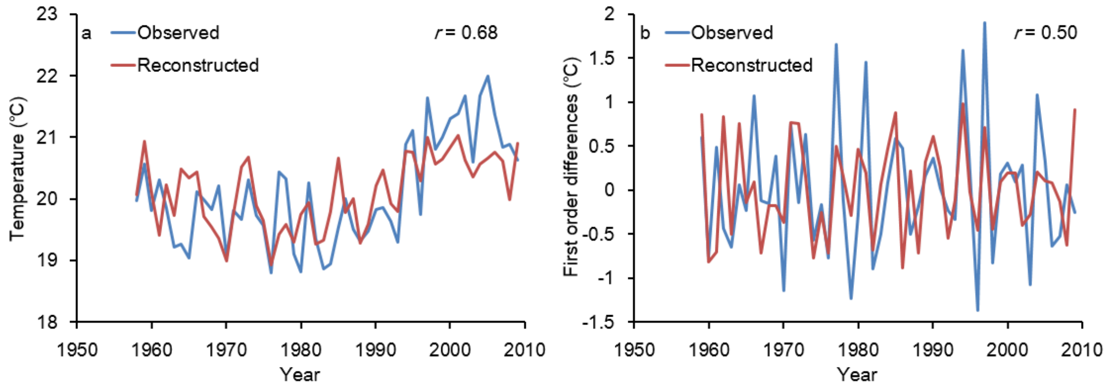

Fig. 3 (a) Comparison between the observed and reconstructed mean March–September temperature of Xi'an for their common period 1958–2009. (b) Comparison between the first differences (year-to-year changes) of actual and reconstructed mean March–September temperature for their common period 1958–2009.

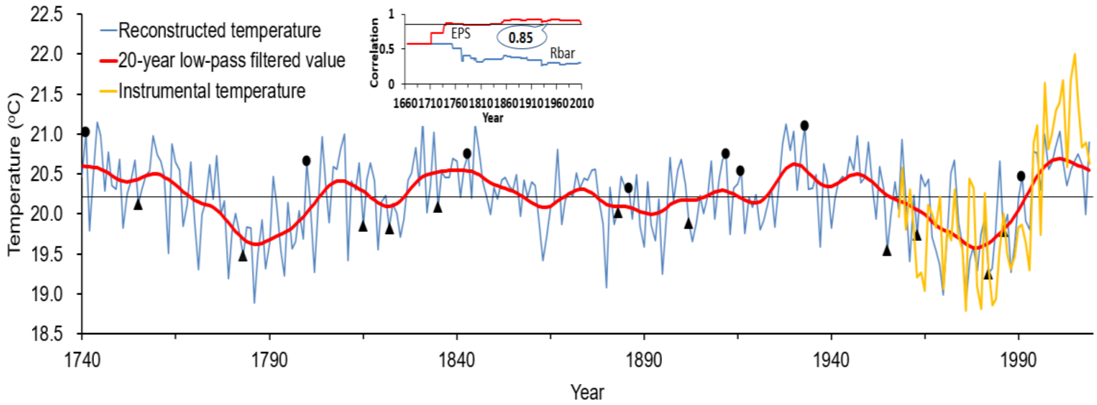

Fig. 4 The March–September temperature reconstruction for the border area (Qingling Mountain) between south and north China plotted annually from 1740 to 2009, along with a 20-year low-pass filtered values (Red thick line). The triangles, and circles indicate volcanic eruption events with cooling in current years and volcanic eruption events (VEI≥ 5) with cooling in the following year, respectively. The small plot showed the EPS and Rbar statistics (calculated over 50 years lagged by 25 years) of the MXD chronology, and the horizontal line represents the 0.85 EPS criterion for signal strength acceptance (Wigley et al 1984).

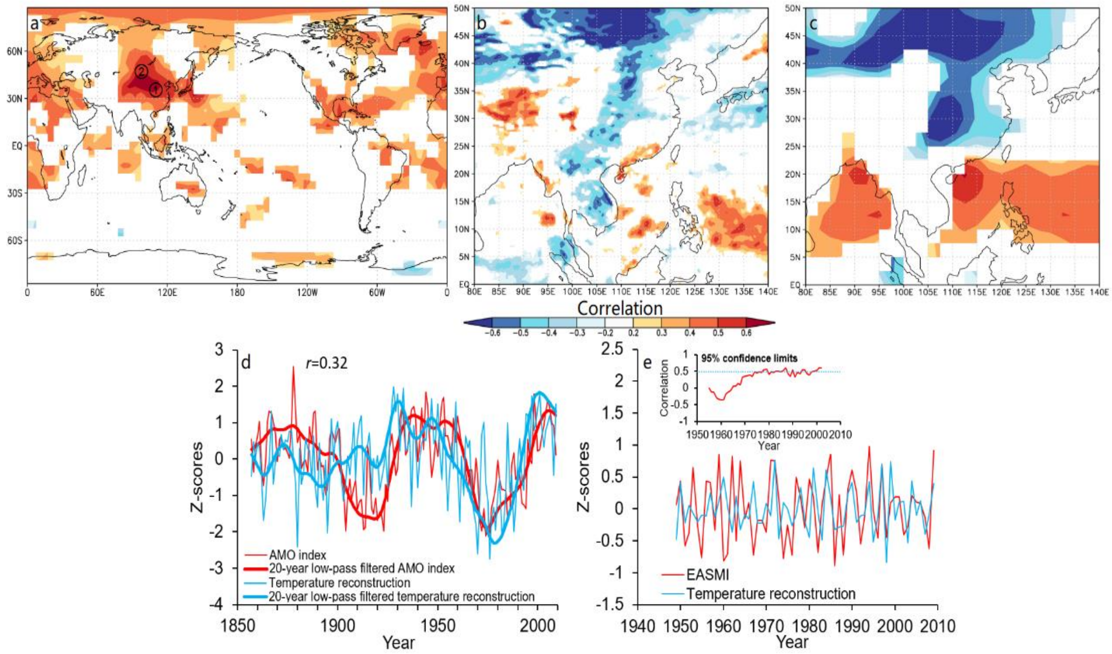

Fig. 5 (a) Spatial correlations of reconstructed March–September temperature with the gridded HadCRUT4/HadSST4 dataset (Cowtan and Way, 2014) for the period 1958–2009. The regions 1 and 2 indicate this study and Hessl et al., 2018, respectively. (b) Spatial correlations of reconstructed March–September temperature with the CFSR precipitation for the period 1979–2009. (c) Spatial correlations of reconstructed March–September temperature with the the CFSR 850mb relative humidity for the period 1979–2009. (d) Comparison of March–September temperature reconstruction in the present study with the AMO index (Enfield et al., 2001). (e) Comparison of the first differences of reconstructed mean March–September temperature and EASMI (Li et al., 2010) for the 1948–2009 period. The insets indicate running 15-year correlation between reconstructed mean March–September temperature and EASMI.

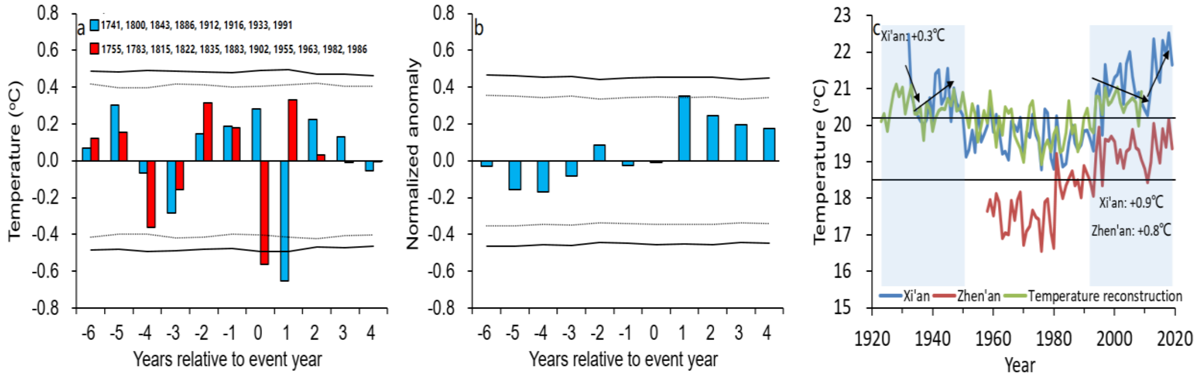

Fig. 6 (a) Results of the superposed epoch analysis (SEA) (Haurwitz and Brier, 1981) between major volcanic events (VEI ≥ 5) and reconstructed March–September temperature. (b) Results of the superposed epoch analysis between all volcanic events (VEI ≥ 5) and the PC1 of the seven drought series of north-central China. The dotted lines and horizontal lines denote the 95% and 99% confidence limits, respectively. (c) Comparison of the actual (Xi'an and Zhen'an) and reconstructed mean March-September temperature for the period 1923–2019.

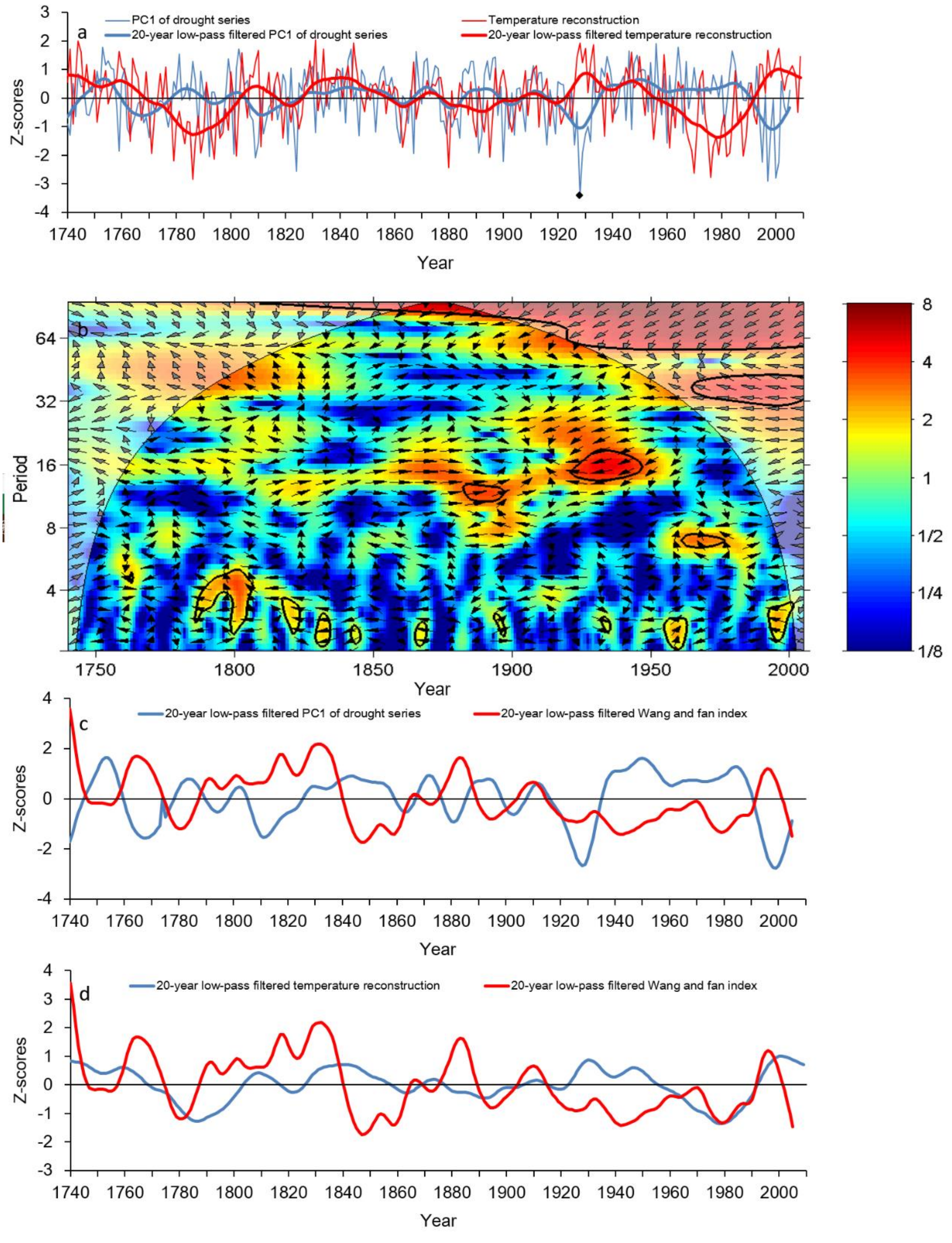

Fig. 7 (a) Graphical comparison of reconstructed March–September temperature and the first principal component (PC1) of the drought sequence of north-central China (Fang et al., 2010, 2012; Chen et al., 2012, 2013, 2014, 2015b, 2016a, b). (b) Cross-wavelet transform of reconstructed March–September temperature and the first principal component (PC1) of the drought sequence of north-central China (Fang et al., 2010, 2012; Chen et al., 2012, 2013, 2014, 2015b, 2016a, b). The 5% significance level against red noise is shown as a thick contour. The arrows showing relative phase of the relationship point to the left for antiphase and to the right for in-phase. The two series were smoothed with a 20-year low-pass filter to indicate the long-term fluctuations. The comparison of EASMI (Wang and Fan, 1999) based on the NCAR's Community Climate System Model 4 (CCSM4) data with (c) the first principal component (PC1) of the drought sequence of north-central China (Fang et al., 2010, 2012; Chen et al., 2012, 2013, 2014, 2015b, 2016a, b) and (d) reconstructed March–September temperature and. The two series were smoothed with a 20-year low-pass filter to indicate the long-term fluctuations.

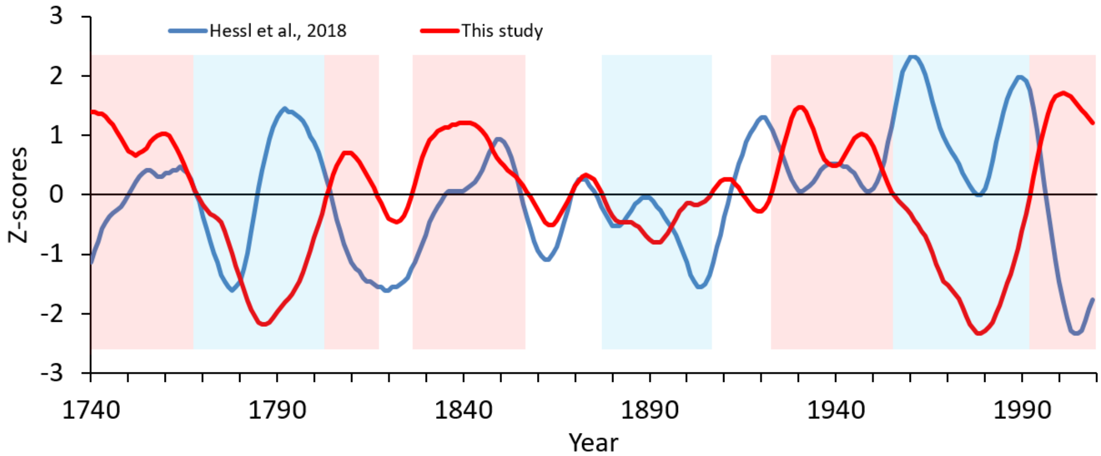

Fig. 8 Graphical comparison of reconstructed March–September temperature and the moisture-sensitive tree-ring width series from Mongolian Plateau (Hessl et al., 2018). Smoothing with a 20-year low-pass filter isolates prominent intervals of high and low streamflow (≥ 15 years). Blue Shadows and red shadows indicate low temperatures and high temperature periods, respectively.